Article

Sedimentary Model and Geological Control of the Ganquan Platform in the Xisha Sea Area, South China Sea

Xuelin Li [1,2], Lei Huang [1,2,*], Kang Lin [2], Mingyuan Sun [2], Jiangyong Zhang [1,2,*], Xining Liu [1,2], Lieyu Tian [2] and Wei Chen [1,2]

1   Sanya Institute of South China Sea Geology, Guangzhou Marine Geological Survey, 2 Yumin Road, Sanya 572025, China; lxlingeo@126.com (X.L.)
2   Guangzhou Marine Geological Survey, China Geological Survey, 1133 Haibin Road, Guangzhou 510075, China; tianlieyu23@163.com (L.T.)
*   Correspondence: lei841004@163.com (L.H.); zjy905@hotmail.com (J.Z.); Tel.: +86-0898-88033822 (L.H. & J.Z.)

Abstract: The Ganquan Platform, located in the South China Sea, exhibits distinctive topographic and geomorphological features shaped by complex geological processes. Utilizing high-resolution multibeam bathymetry and multi-channel seismic data, this study provides a comprehensive investigation into the sedimentary evolution and stratigraphic framework of the platform. Morphologically, the platform is identified as an elongated seamount, with water depths ranging from 530 m to 800 m and a maximum elevation of 538.115 m. Seismic facies analysis reveals seven distinct facies, reflecting a dynamic and intricate history of carbonate deposition. The stratigraphic framework delineates three primary evolutionary stages: the growth phase (Early Miocene), characterized by the initial accumulation of carbonate sediments; the flourishing phase (Middle Miocene), marked by extensive deposition and platform expansion; and the submergence phase (Late Miocene), defined by progressive submersion and erosion of carbonate features. This evolutionary trajectory was driven by key factors such as terrigenous clastic input, tectonic activity, sea-level fluctuations, and paleoenvironmental dynamics. The findings contribute to a deeper understanding of the Ganquan Platform's geological history and its role in the broader context of submarine geology in the Xisha region.

Keywords: Ganquan Platform; sedimentary evolution; seismic facies; stratigraphic characteristics; geological control

1. Introduction

Bioherms refer to the carbonate buildups formed by the in situ growth of attached benthic reef-building organisms, with large bioherms forming carbonate platforms. Carbonate platforms with reefs predominantly grow in tropical to subtropical marine environments within 30° latitude of the equator [1]. Carbonate platforms are categorized into three types based on their morphology, scale, and proximity to land: ramp platforms, rimmed shelf-edge platforms, and isolated platforms. Carbonate platforms are classified into modern carbonate platforms and submerged carbonate platforms, depending on their current state of development [2]. Buried reefs within the stratigraphy of carbonate platforms are classified by shape into pinnacle reefs, tower reefs, horseshoe reefs, atolls, bioherms, and stratiform reefs [3].

The sedimentary evolution process and controlling factors of biohermal carbonate platforms have been key research focuses in recent years. Extensive research on biohermal carbonate platforms has been conducted in key regions, including the Bahamas Banks, the Maldives, the Northwest Shelf of Australia, the Great Barrier Reef, and Southeast Asia. Recent findings indicate that the slope deposits along the margins of the Bahamas platform are composite formations resulting from multiple phases of small-scale, intermittent gravity flows [4]. The successful completion of IODP Expedition 381 has provided significant insights, revealing that the evolution of the Maldives carbonate platform is intricately linked

to tectonic activity and monsoonal dynamics [5]. Meanwhile, carbonate platforms in Southeast Asia and offshore Australia are classified as tropical humid carbonate systems, where equatorial tropical conditions exert a profound influence on the carbonate sedimentary framework. Key factors driving the development of these platforms include monsoonal climate patterns, the input of terrigenous materials, and elevated nutrient levels [6]. The South China Sea hosts numerous carbonate platforms, primarily concentrated in the Nansha, Xisha, Zhongsha, and Dongsha regions [7]. With the advancement of deep-water oil and gas exploration, the understanding of the distribution of carbonate platforms in the South China Sea has become increasingly refined. During the Miocene, carbonate platforms were more extensively distributed across the region [7,8]. Researchers have identified large carbonate platforms in the southern South China Sea, including the Malampaya [9], Beikang [10], Nanwei [11], Liyue [12], and Wan'an platforms [13]. In the northern region, notable platforms such as Liuhua [14], Xisha [15], Guangle [16], and Baodao [17] have been discovered. Significant bioherm-associated oil and gas fields have been found in the Zengmu [18], Wan'an [19], and North Palawan basins [20] in the south, as well as the Liyue and Pearl River Mouth basins [21] in the north. These carbonate platforms reached their maximum extent by the end of the Early Miocene, after which their size gradually diminished, with bioherms now primarily developing on localized elevated areas [7,8].

In recent years, the sedimentary processes of carbonate platforms in the South China Sea and their links to regional tectonic activity, relative sea level fluctuations, climate change, and oceanic current variations have been increasingly deciphered [17,22–27]. These insights underscore the critical scientific significance of South China Sea carbonate platforms in understanding the tectonic evolution of the continental margin, paleo-sea level variations, and ancient oceanic and climatic environments. Previous studies, utilizing data from multiple wells [28,29] and multi-channel seismic surveys [15,30], have established a sequence stratigraphic framework for the Xisha carbonate platform and analyzed its stratigraphic characteristics. The development of the Xisha carbonate platform commenced in the Late Oligocene, with its evolution largely governed by regional tectonic subsidence and relative sea-level changes. Carbonate sedimentation reached its peak during the Middle Miocene, but with the rapid rise in sea levels, most platforms were gradually submerged, becoming known as submerged carbonate platforms. Only the Xuande and Yongle atolls have continued to develop into the present, forming modern island reef systems [31,32].

Recent research on the Xisha carbonate platform has primarily focused on the sedimentary models, development, evolution, and controlling factors of modern islands and reefs [31,33]. In contrast, the submerged carbonate platforms of Xisha are more extensively distributed than the modern reefs, yet their stratigraphic structures and sedimentary processes remain poorly understood. This gap in knowledge makes it difficult to investigate the mechanisms that control the development and eventual submergence of these platforms.

The Ganquan Platform, located at the edge of the Xisha Uplift (Figure 1), serves as a typical example of a submerged carbonate platform, significantly influenced by hydrodynamic changes [34]. This study selects the Ganquan Platform as the research target, utilizing multibeam bathymetric data and newly acquired high-resolution multi-channel seismic data. Building upon the sequence stratigraphic framework established in previous studies of the Xisha region and incorporating existing drilling data and relative sea level change records, this research conducts seismic sequence and sequence stratigraphy analysis to delineate the stratigraphic structure of the Ganquan Platform. The study further explores the platform's developmental evolution and the factors that have influenced its growth and submergence.
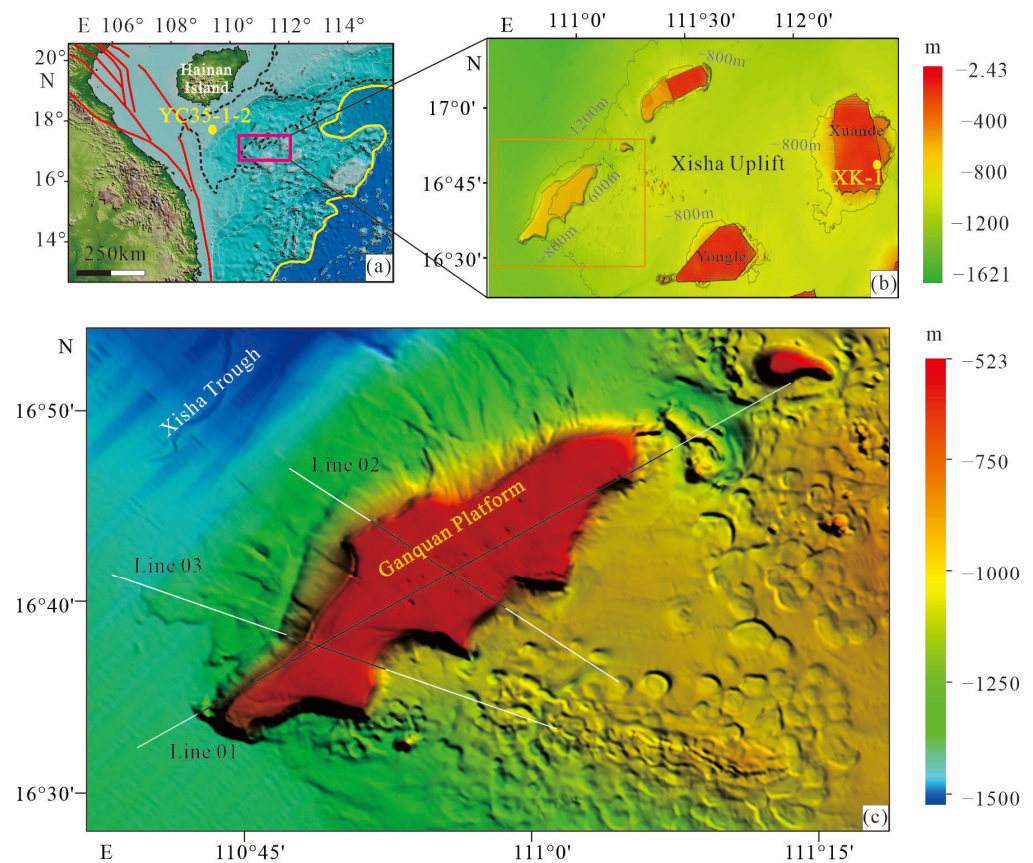
Figure 1. (**a**) represents the tectonic background map of the northwestern South China Sea, (**b**) represents the bathymetric map of the Xisha area, and (**c**) represents the topographic and geomorphological map of the study area. In map (**a**), the red solid lines indicate faults, the yellow dots represent YC-35-1-2, and the pink box marks the location of map (**b**). In map (**b**), the yellow dots represent XK-1, and the orange box marks the location of map (**c**). In map (**c**), The white solid lines represent the positions of seismic profiles outside the platform (which are not covered in this study), while the black solid lines represent the seismic profiles that cut through the platform.

2. Geological Background

The South China Sea is the largest marginal sea in East Asia, formed through rifting and seafloor spreading that occurred between the Late Cretaceous and Early Oligocene [35,36]. The Xisha Uplift is a significant tectonic unit in the northwestern South China Sea. To the north, it is separated from the South China Block by the Xisha Trough; to the east, it borders the Northwestern Sub-basin of the South China Sea; to the southeast, it is divided from the Zhongsha Block by the Zhongsha Trough; to the south, it adjoins the Southwestern Sub-basin; and to the west, it faces the Indochina Block, with strike-slip faults developed between them. Since the Late Cretaceous, the Xisha Uplift has experienced two distinct stages: a rifting phase and a thermal subsidence phase [37]. The rifting phase primarily occurred during the Paleogene, and in the later stages, volcanic activity was frequent in the Xisha Uplift. The top of the uplift fractured, forming multiple volcanic uplifts and fault-controlled tectonic highs [38]. Beginning in the Early Miocene, the Xisha Uplift entered the thermal subsidence phase. During this period, bioherms and carbonate platforms began to develop on the uplifted blocks formed during the rifting phase [39]. The thermal subsidence also facilitated the upwelling and escape of fluids and gases from the Xisha Uplift through the seabed, resulting in the formation of various types of pockmarks [34]. Data from Well XK-1 shows that the basement of the Xisha Uplift is composed of granite, granitic gneiss, and basalt [40,41], indicating a history of magmatic activity and metamorphism in the basement [42].

Since the Neogene, the relative sea level of the Xisha Uplift has undergone multiple fluctuations (Figure 2). In the Early Miocene, the relative sea level gradually rose, followed by a decline from the Late Early Miocene to the Late Miocene. From the Late Miocene to the Pliocene, the sea level rose rapidly, then declined again after the Pliocene [29]. Since the Neogene, the monsoon influence on the Xisha Uplift has intensified three times, around 15 Ma, 8 Ma, and 3 Ma [43].
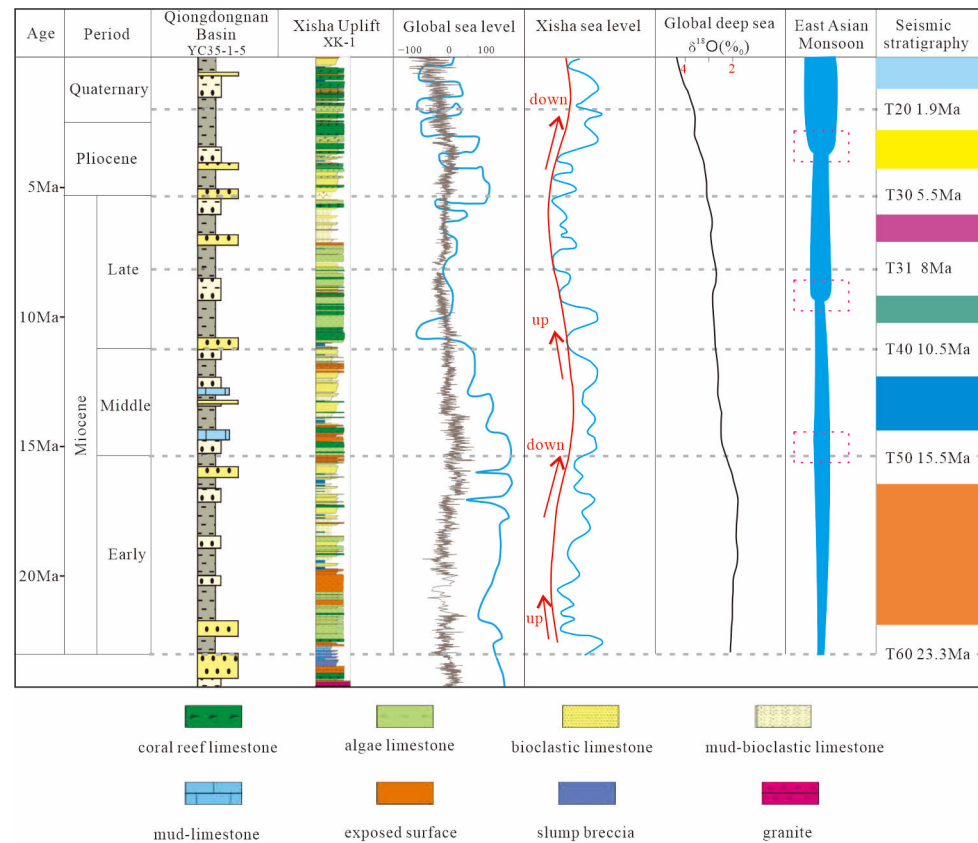
Figure 2. Comparison chart of stratigraphic structure, sea level changes, and East Asian monsoon variations. Well YC35-1-2 modified from [44], Well XK-1 modified from [40]. Global sea level changes based on [45,46], δ18O and East Asian monsoon based on [43], and seismic sequences based on regional stratigraphic interpretations of the Qiongdongnan Basin and Xisha carbonate platforms [15].

The Ganquan Platform is located at the western edge of the Xisha Uplift and is a typical submerged platform, extending in a northeast–southwest elongated shape. To the east of the Ganquan Platform lie the Xuande and Yongle Atolls, two major modern carbonate platforms. Drilling data indicate that the carbonate strata above the platform's basement exceed 1200 m in thickness.

3. Materials and Methods

This study primarily utilizes 3000 km^2 of multibeam bathymetric data and 350 km of high-resolution multi-channel seismic data. The multibeam bathymetric data, provided by the Guangzhou Marine Geological Survey, have a resolution of 50 m × 50 m and were used to construct the topographic and geomorphological map of the Ganquan Platform (Figure 1c). The seismic data for Line 3 (approximately 15 km, Figure 1c) were sourced from [47], while the remaining 335 km of seismic data were provided by the Guangzhou Marine Geological Survey. These 335 km of seismic data were acquired using a single-side excitation and reception, non-zero offset, single-cable observation system, with an air gun as the seismic source. The raw seismic data underwent processing through a seismic data processing system, which included noise suppression, multiple attenuation, velocity analy-

sis, pre-stack time migration, and post-processing. Noise suppression primarily employed low-cut filtering to reduce strong surge noise, while the AAA technique was applied to attenuate anomalous amplitude noise. Multiple attenuation was handled using a multi-step serial approach (SRME + RADON transform + RES_DEMUL), effectively suppressing most multiples and significantly enhancing the signal-to-noise ratio of the profiles, which greatly benefited subsequent migration processing. Velocity analysis was iterated three times, selecting appropriate velocities for multiple attenuation, stacking, and migration. The velocity field changes were consistent with geological variations, following the principles of accurate velocity spectrum picking, common midpoint gather flattening, geological coherence, and focused imaging. Kirchhoff pre-stack time migration was applied to achieve accurate stratigraphic positioning. Post-processing was then performed on the migrated stacked profiles, enhancing visualization while adhering to the principles of preserving effective reflections, maintaining wavelet characteristics, and retaining amplitude fidelity. The processed seismic data were interpreted using the Petrel 2024 E&P software platform.

Sequence stratigraphy, by integrating time and relative sea-level changes to track facies shifts, is considered an effective method for analyzing the development history of carbonate platforms. Carbonate sequence stratigraphy shares some similarities with clastic sequence stratigraphy. Sequence boundaries in both types of stratigraphy exhibit conformable and unconformable contacts. Unconformable contacts typically indicate sedimentary interruptions, showing features such as onlap and erosion in profiles. However, there are also differences. Deposition on carbonate platforms in the South China Sea is mainly chemical and biogenic, with mechanical deposition occurring primarily in areas with strong hydrodynamics and short transport distances. Therefore, carbonate buildups on seismic profiles of carbonate platforms exhibit different patterns in terms of topography and geomorphology compared to clastic rocks [48]. In this study, we combined the stratigraphic framework established by previous researchers in the Xisha area (Figure 2) with seismic facies characteristics, interpreting seismic profile and multibeam bathymetric data (Figure 1), to establish the sedimentary model of the Ganquan Platform.

4. Results

4.1. Interpretation of Multibeam Bathymetry Data

The Ganquan Platform has the shape of an elongated seamount in the northwest–southeast direction, with a long axis of approximately 46 km, a short axis of about 12 km, and an area of around 300 km^2. The water depth at the top of the platform ranges from about 800 m to 530 m, with depths greater than 600 m in the southeast, while depths in the central and northwest parts are mostly less than 600 m. The highest point of the platform is 538.115 m. The top of the platform is flat, with a maximum slope of no more than 3°. There are several circular sinkholes on the platform's top (Figure 3), associated with magmatic activity [49].

The topography of the slopes on the northwest and southeast sides of the Ganquan Platform is complex and distinct. On the northwest slope, sedimentary slump deposits surround the foot of the slope, forming a slope apron. Above this apron, several irregularly developed channels of varying scales can be observed, with depths ranging from 5 to 75 m (Figure 3). The larger channels are connected to the Xisha Trough, serving as conduits for transporting sediments toward the trough. In contrast, the southeast slope does not exhibit slumps or channel development; however, at the distal end of the slope, clusters or groups of pockmarks have developed, which are related to gas escape from the deeper strata [34].
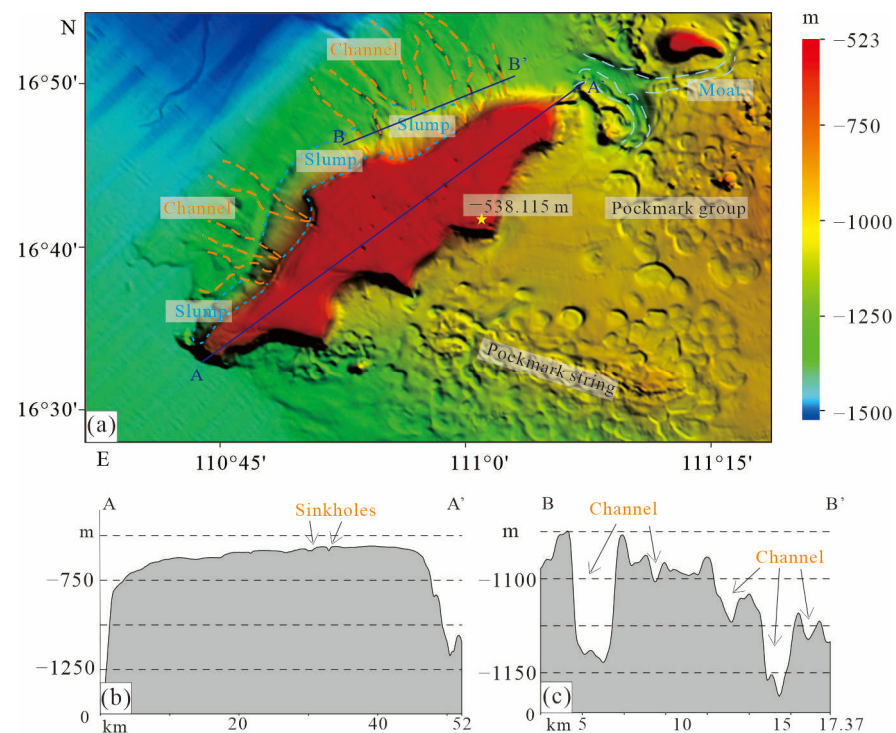
Figure 3. (**a**) Topographic and geomorphological map of the Ganquan Platform and surrounding sea areas. The orange dashed line indicates the channels and the blue dashed line indicates the slumps. The dark blue solid line represents the cross-sections in AA' and BB', The yellow star indicates the location of the highest point. The light blue long dashed line indicates the moat. (**b**) is the bathymetric profile across the platform in the southwest-northeast direction. (**c**) is the bathymetric profile across the channel and slump in the northwestern part of the platform.

4.2. Interpretation of Multi-Channel Reflection Seismic Data

4.2.1. Seismic Facies

Different geological bodies exhibit variations in their reflection characteristics on seismic profiles, such as amplitude, continuity, morphology, and internal features [3,33]. By comparing the lithofacies from Well XK-1 and analyzing the seismic characteristics of the Ganquan Platform, seven distinct seismic facies have been identified in the seismic profiles, as detailed in Table 1. Within the platform, extensive lagoonal facies are present, characterized by moderately continuous, low to moderate amplitude, wavy-horizontal parallel reflections. Karst topography is also identified within the platform, exhibiting parallel and moderately continuous features in the seismic isochron, with higher amplitudes. Progradational facies have been recognized at the platform edge, displaying higher amplitudes and S-shaped parallel reflections that onlap the underlying strata. In the deeper parts of the platform, biogenic reefs have been identified, characterized by medium amplitude and upward-arching isochrons, with chaotic reflections internally. Surrounding the biogenic reefs, debris has been identified, with reflection characteristics of moderate-to-strong amplitude and weak continuity. The platform is encircled by a reef rim, which exhibits seismic facies characterized by weak amplitude, moderate continuity, and a convex-up shape. Gas chimneys have developed within the platform, typically penetrating through the entire carbonate layer, characterized by chaotic reflections, weak continuity, and a vertical wedge-shaped morphology in the seismic profiles.

Table 1. Seismic facies description and interpretation summary.

Seismic Facies(s)	Reflection Characteristics	Interpretation
	Moderately continuous, low to moderate amplitude, wavy-horizontal parallel reflections	Lagoon
	Moderately continuous, high amplitude, parallel reflections	Karst
	Onlap, moderate to high amplitude, S-shaped subparallel reflections	Carbonate platform progradation margin
	Upward convex moderate amplitude reflections with chaotic internal reflections	Biogenic reef
	Moderate-to-strong amplitude, weak continuity, chaotic reflections	Debris
	Chaotic reflections, weak continuity, vertical wedge-shaped	Gas chimney
	Weak amplitude, moderate continuity, convex-up shape	Reef rim
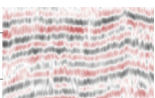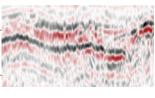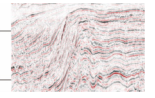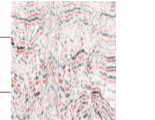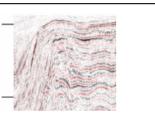
4.2.2. Sequence Stratigraphy Division and Stratigraphic Characteristics

Based on the previously established sequence stratigraphy framework for the Xisha Sea area and sea level changes (Figure 2), a sequence stratigraphic analysis of the Ganquan Platform's high-resolution multi-channel seismic data was conducted, identifying four sequence boundaries. Referring to drilling data from the Xisha Sea area (Figure 2), these boundaries are interpreted as the Early Miocene base T60, the Middle Miocene base T50, the Late Miocene base T40, and the Late Miocene T31 (Figures 4 and 5).

Early Miocene sequence (T60–T50). The Early Miocene sequence of the Ganquan Platform developed as a product of the thermal subsidence phase, significantly eroded in volcanic uplift areas or tectonic highs. The top of the Early Miocene sequence, T60, is characterized by relatively high overall frequency, strong amplitude, and good continuity. The base T50 boundary exhibits moderate frequency, weak-to-moderate amplitude, and good continuity. Overall, the seismic facies of the Early Miocene sequence feature sheet-like, subparallel, moderate-to-weak amplitude, medium-low frequency, and moderate-to-weak continuous reflections.

The Middle Miocene sequence (T50–T40) represents the sedimentary products of the subsidence phase. The top of the Middle Miocene sequence, T40, is characterized by medium-to-strong amplitude, high frequency, high continuity, and biphasic seismic reflections, exhibiting onlap truncation in tectonic high areas. Overall, the seismic facies of the Middle Miocene sequence feature subparallel, medium-to-low amplitude, medium frequency, and medium-to-high continuity reflections, with increased frequency and improved continuity of internal reflection wave groups compared to the Early Miocene sequence.

In the seismic profile crossing the northwestern part of the Ganquan Platform, two progradational tops, T41 and T42, are identified within the Middle Miocene sequence (T50–T40). Both T41 and T42 exhibit onlap relationships with the underlying strata, and

the seismic facies show moderate to high amplitude and moderately continuous reflections. The sequences delineated by these two progradational tops exhibit overall moderate-to-strong amplitude, weak continuity, and chaotic reflections (Figure 6).
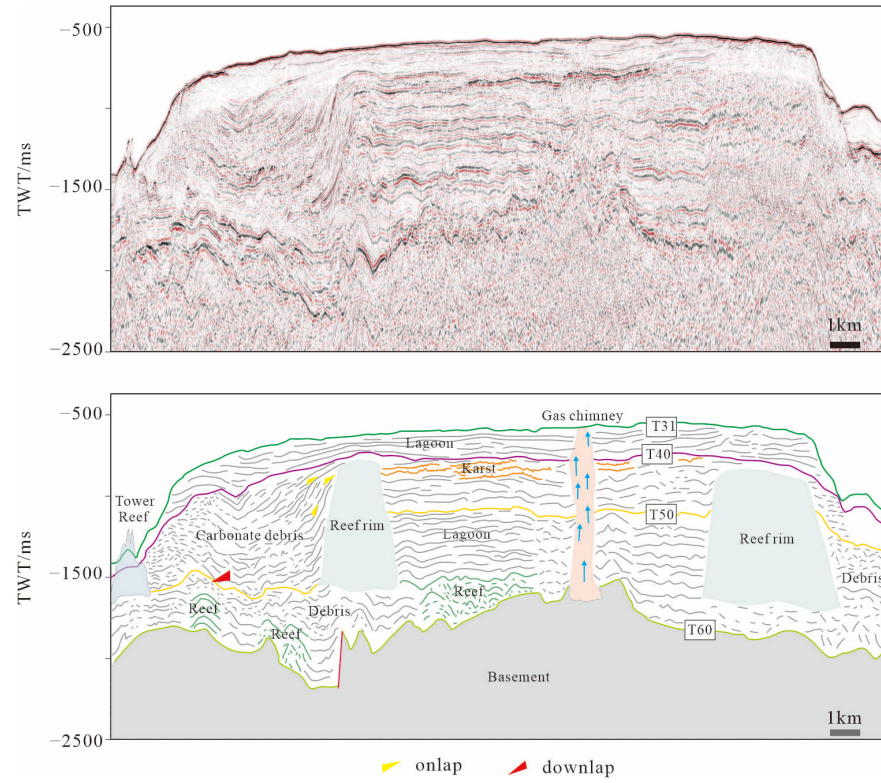
Figure 4. Seismic profile of Line 01 (**upper**) and interpretation (**lower**).
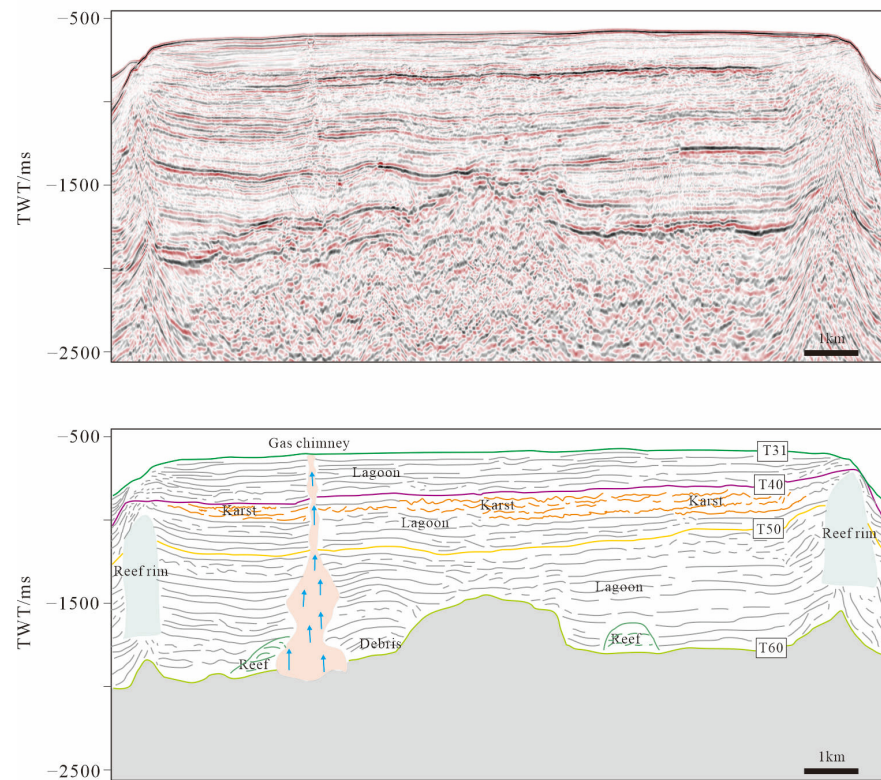
Figure 5. Seismic profile of Line 02 (**upper**) and interpretation (**lower**).
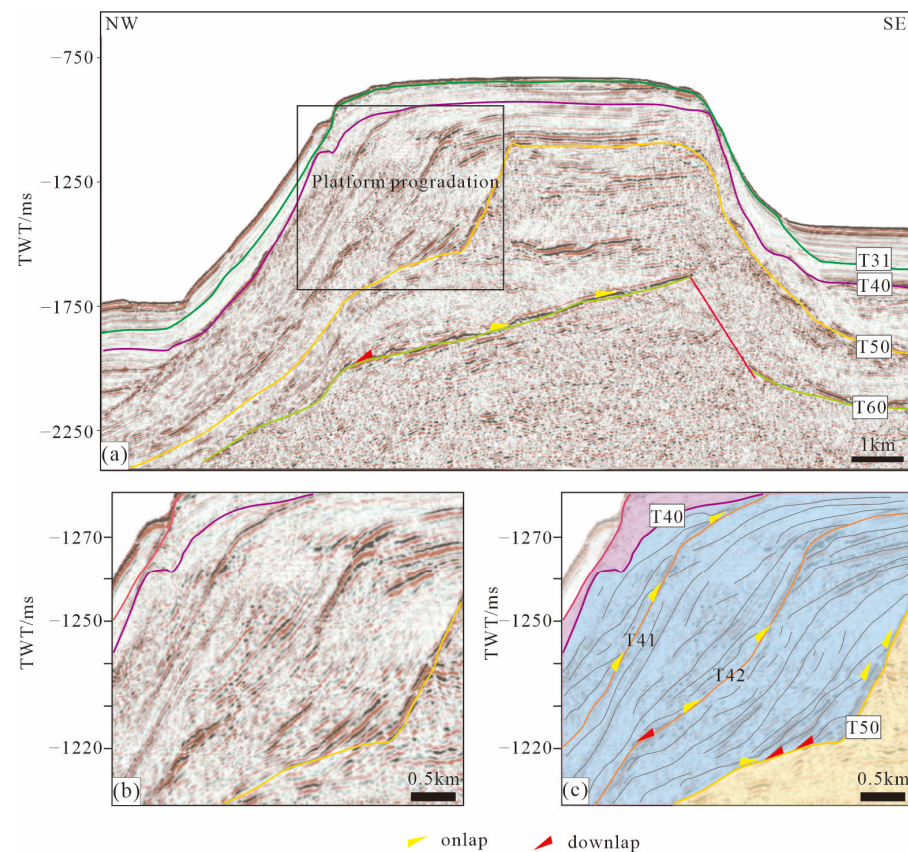
Figure 6. (**a**) is the seismic profile of Line 03. The black box represents the platform progradation and the red solid line indicates the fault. (**b**) is an enlarged view of the seismic profile of the platform progradation. (**c**) is a detailed explanation of the sequence stratigraphy of the platform progradation.

The Late Miocene sequence (T40–T31) represents the sedimentary products of the regional subsidence phase. The T31 boundary marks the top of the Late Miocene sequence and also serves as the upper boundary of the Ganquan Platform, exhibiting high amplitude, medium to low frequency, and medium to high continuity in its seismic reflections. Overall, the seismic facies of the Late Miocene sequence are characterized by high amplitude, high frequency, and medium to high continuity reflections. The reflections generally appear relatively flat and stable while locally displaying chaotic and blank seismic reflections.

4.3. Stratigraphic Characteristics of the Ganquan Platform

Well XK-1 data shows that the Xisha area has deposited nearly 1300 m of carbonate rock layers since the Middle Miocene. The latest sampling survey results indicate that sporadic loose sediments of about 4 m thickness are present at the top of the Ganquan Platform, with most areas being exposed carbonate rock layers [47]. Combined with the seismic profile of the Ganquan Platform, it is believed that the strata above T60 are all carbonate rock layers. The seismic profile shows that the Ganquan Platform has developed a 0.6 s carbonate rock layer in the time domain (Figure 4). Roughly converting the time to depth, with a velocity of 2500 m/s for the carbonate rock layer in the platform area [26], it is estimated that the Ganquan Platform has grown approximately 700 m of biogenic reef carbonate rock layers since the Miocene.

Comparing the data from Well XK-1 with the relative sea-level change curve of the Xisha region (Figure 2), the seismic data indicate that the carbonate rock layers of the platform area mainly exhibit lagoon facies, with karst development commonly observed at the top boundaries of the Middle Miocene. The presence of a gas chimney suggests continuous fluid upwelling and erosion within the platform interior. In the early Early Miocene, reefs began to sporadically grow at tectonic highs, while the surrounding low-lying areas began

to accumulate mixed sedimentary deposits of siliciclastic and carbonate debris. Seismic reflections in deeper zones exhibit higher amplitudes, suggesting a higher content of siliciclastic debris, while reflections in shallower zones show lower amplitudes, indicating a higher content of carbonate rock debris. In the Middle Miocene strata of the northwestern Ganquan Platform, two progradational events occurred, with the progradational sediments primarily consisting of carbonate debris.

5. Discussion

5.1. Sedimentary Model of Ganquan Platform

Based on the stratigraphic characteristics of the Ganquan Platform and the tectonic background of the Xisha region, a sedimentary model for the Ganquan Platform has been established. It is proposed that the sedimentary evolution of the Ganquan Platform can be divided into three stages: the Early Miocene, during which carbonate rocks began to deposit and gradually formed the platform, referred to as the growth phase; the Middle Miocene, characterized by extensive deposition of carbonate rocks, leading to the expansion and deepening of the platform, known as the flourishing phase; and the Late Miocene, when the deposition of carbonate rocks slowed, causing the platform to gradually shrink until it was submerged, referred to as the submergence phase (Figure 7).
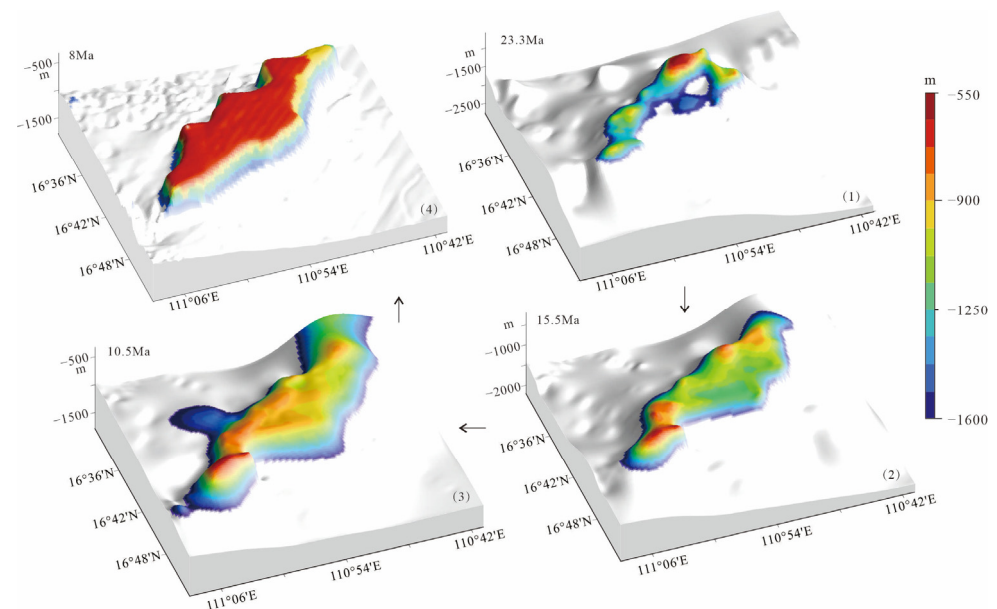
Figure 7. The sedimentary evolution process of the Ganquan Sea Platform since 23.3 Ma. The colored area represents carbonate rock deposition, and the gray area indicates the semi-neritic to oceanic region. (**1**) Indicates that carbonate rocks were deposited only on tectonic highs at 23.3 Ma. (**2**) Indicates that at 15.5 Ma, carbonate rocks developed on a large scale to form a platform. (**3**) Indicates that at 10.5 Ma, the platform prograded outward, expanding in area. (**4**) Shows that after 8 Ma, carbonate rock deposition ceased.

5.1.1. Growth Phase (Early Miocene)

During the Late Oligocene to Early Miocene, some low-lying areas began to grow biogenic reefs, while the bedrock of elevated points remained exposed above the sea level. Strong dynamic marine currents eroded and transported the biogenic reefs in the low-lying areas and the bedrock at elevated points. During this period, sedimentation was primarily characterized by a mixture of siliceous and carbonate debris. Entering the Early Miocene, the entire region of Xisha was submerged, with elevated points being submerged [50], initiating extensive growth of biogenic reefs. Low-lying areas were below the photic zone, ceasing the in situ growth of biogenic reefs, with sedimentation primarily composed of carbonate debris transported from elevated points, mixed with a small amount

of siliceous debris. With the continuous stable rise of sea levels, biogenic reefs proliferated and accumulated significantly at elevated points, developing into carbonate platforms. By the end of the Early Miocene, carbonate platforms had begun to take shape on a substantial scale.

5.1.2. Flourishing Phase (Middle Miocene)

During the Middle Miocene, the secondary fluctuations in relative sea level showed an upward trend, providing accommodation space for the vertical growth of carbonate platforms, resulting in the thickening of the carbonate strata of the Ganquan Platform. However, the frequent alternation of tertiary fluctuations in relative sea level [29] led to a more complex sedimentary process on the Ganquan Platform. When the tertiary fluctuations were in a downward trend, the vertical deposition of carbonate rocks ceased, causing shallower water depths at the top of the platform. Enhanced tidal erosion damaged the carbonate rocks at the platform's summit, generating carbonate debris that was transported to the platform slope, and facilitating horizontal growth and area expansion. During the Miocene, there were two significant declines in tertiary sea level, corresponding to two progradational events on the Ganquan Platform. The second major decline in sea level caused the platform's summit to emerge above sea level, resulting in the formation of karst landforms.

5.1.3. Submergence Phase (Late Miocene)

In the early Late Miocene, relative sea levels rose slowly, allowing the platform to grow steadily in sync with the sea level. The slopes at the edges of the platform transitioned into a bathyal environment, and the Ganquan Platform developed into an isolated carbonate platform. In the mid-Late Miocene, relative sea levels rose rapidly, causing the top of the platform to gradually fall below the photic zone, leading to the decline of reef-forming organisms. The rate of carbonate deposition could not keep pace with the rising relative sea level, resulting in gradual submergence. As relative sea levels continued to rise, the Ganquan Platform reached its current underwater state of 500 to 800 m. Ocean currents persistently eroded the edges and surface of the platform, and the exposed bioherms at the top of the platform were gradually eroded, leading to a flattening of the surface. The slopes of the platform transitioned into deeper water, with significant development of carbonate debris gravity flows, and contour currents developed along the slopes, primarily characterized by finer-grained contour current deposits [51].

5.2. Factors Controlling the Stratigraphic Evolution of the Ganquan Platform

Based on previous studies of various types of ancient and modern carbonate platforms and their controlling factors globally [25,52,53], and by comparing the changes in the ancient sedimentary environment of the Ganquan Platform region, the factors influencing the evolution of the Ganquan Platform are analyzed. The main factors controlling the development and evolution of carbonate platforms include five major aspects: (1) input of terrigenous clastic materials; (2) tectonic activity; (3) changes in sea level; and (4) variations in paleomonsoons and paleocurrents.

5.2.1. The Impact of Terrigenous Clastic Input on the Ganquan Platform

From the perspective of tectonic evolution in the Xisha Sea region, there were significant differences in tectonic subsidence from 32 to 23.3 Ma. The ancient subsidence in the Xisha Uplift was much less than in the surrounding areas, where large-scale subsidence led to the formation of deep-water basins such as the Xisha Trough, Qiongdongnan Basin, and Zhongjian Nan Basin prior to the Miocene [15]. Terrigenous clastic materials from the South China Block and the Indochina Peninsula were transported to these basins, where they settled due to weakened hydrodynamic conditions and could not reach the Xisha Uplift area. Consequently, the Ganquan Platform region exhibited a clean water environ-

ment, providing a suitable setting for the later growth of bioherms and the development of carbonate platforms.

With the onset of the Miocene, the Ganquan Platform began to accumulate carbonate rocks, while the surrounding basins continued to experience rapid subsidence, deepening the waters of tectonic units like the Xisha Trough and further preventing terrigenous materials from reaching the areas where carbonate platforms were developing. Although terrigenous clastic input can inhibit coral growth, thereby affecting carbonate deposition and platform development, the absence of terrigenous clastic input since the Miocene has meant that it has had little to no impact on the development of the Ganquan Platform.

5.2.2. The Impact of Tectonic Activity and Sea Level Changes on the Ganquan Platform

There was a significant transformation in tectonic activity in the Xisha area, marked by the Miocene boundary. Before the Miocene, the region was in a rifting phase, characterized by extensive fault activity, making it unsuitable for carbonate deposition as the growth of bioherms requires a stable tectonic environment. Beginning in the Miocene, the area entered a post-rift phase dominated by stable thermal subsidence, providing a foundation for the development of carbonate platforms on the Ganquan Platform. From 23.3 Ma to 8 Ma, the rate of thermal subsidence gradually increased (Figure 8), leading to a slow rise in relative sea levels and creating suitable accommodation space for carbonate platform development. After 8 Ma, the rate of tectonic sedimentation surged dramatically, causing a rapid rise in relative sea levels (Figure 8), which ultimately led to the submergence of the Ganquan Platform.
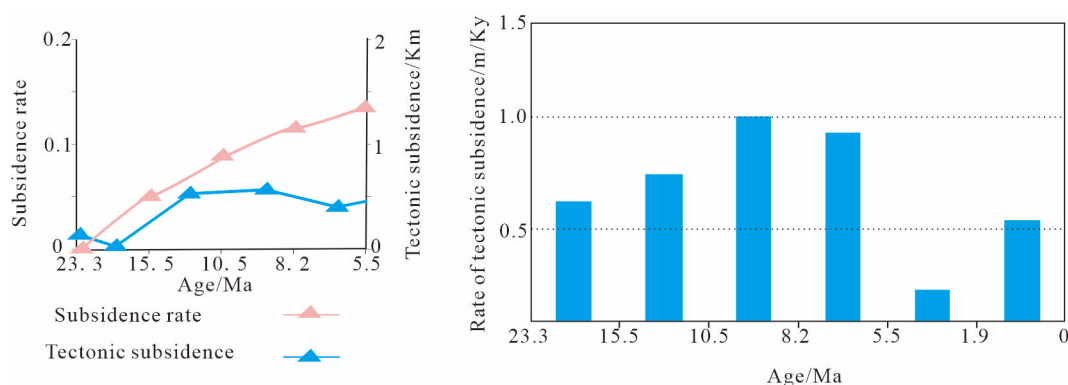
Figure 8. Subsidence rate and amount of subsidence of the Xisha Uplift.

Tectonic subsidence and global sea level fluctuations jointly influence relative sea level changes in the Xisha area. Since the Miocene, the second-order cycles of relative sea level in the Xisha area have shown an upward trend, while the third-order cycles exhibit multi-phase periodic characteristics at different times. As the overall relative sea level rose in the early Miocene, the entire Ganquan Platform was submerged, allowing for its gradual and prosperous development. The two declines in the third-order relative sea level changes during the Middle Miocene eroded the top of the Ganquan Platform, resulting in relatively thin carbonate deposits from this period. The substantial carbonate debris eroded from the top was transported to the slope, shallowing the water depth and bringing the area into the photic zone, where bioherms began to develop, ultimately leading to an expansion of the platform area. During the Late Miocene, the acceleration of the relative sea level rise caused the entire Ganquan Platform to remain submerged beneath the photic zone.

5.2.3. The Impact of Paleomonsoons and Paleocurrents on the Ganquan Platform

Monsoons can drive the movement of surface seawater, and when the monsoon intensity increases in the area of the carbonate platform, the velocity of surface currents also accelerates. This acceleration leads to two main outcomes. First, the increased surface current speed enhances the erosive capacity of seawater on the platform's top, resulting in

greater destruction of previously grown reefs and deposited carbonate rocks, which are then transformed into carbonate clasts. Under the influence of tidal forces and gravity, these clasts are transported to the leeward slope, causing the slope of the leeward side to be less steep than that of the windward side, resulting in a greater sediment thickness on the leeward slope [54]. Second, the faster surface currents reduce the pressure of surface seawater, causing deeper waters, which move slower, to rise and create upwelling and turbulence. These upwellings and turbulence can bring nutrient-rich deep water to the platform's top, which may inhibit the growth of reefs [25] (Figure 9).
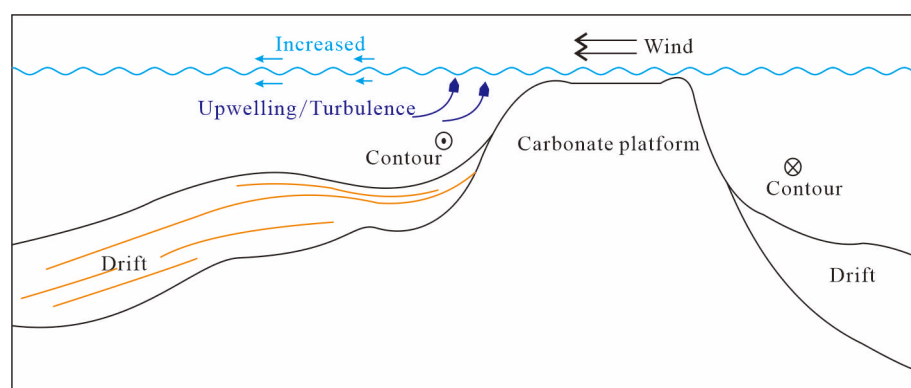
Figure 9. The model of monsoon and ocean currents' affection to the platform deposition, modified according to [25].

After 21 Ma, the South China Sea developed the East Asian monsoon. Driven by wind, surface seawater is influenced by the Coriolis effect in the Northern Hemisphere, causing its flow direction to veer to the right of the wind direction. In winter, the flow moves from the northeast to the southwest, while in summer, it shifts from the southwest to the northeast, with the northern South China Sea experiencing more intense winter monsoon effects [55]. Previous studies indicate that the intensity of the East Asian monsoon, which began in the early Miocene, experienced two strengthening events at 15 Ma and 8 Ma, with the 15 Ma event being relatively minor and the 8 Ma event being significantly stronger [43]. These two strengthening phases accelerated the flow of surface seawater toward the southwest in the Ganquan Platform region. The 15 Ma monsoon enhancement contributed to the erosion of carbonate rocks on the top of the platform, transporting them to the leeward slope and expanding the area of the platform. The sharp increase in monsoon intensity at 8 Ma, combined with the rapid rise in relative sea level, led to the submergence of the platform.

6. Conclusions

(1) Through high-resolution multibeam and seismic data, we identified key stratigraphic features of the Ganquan Platform, including lagoonal facies, karst formations, and biogenic reefs. The carbonate rock layers, primarily developed since the Miocene, reflect the complex interplay of tectonic stability and sea-level changes that facilitated the platform's evolution.

(2) We present the sedimentary evolution of the Ganquan Platform, identifying distinct phases: the Early Miocene growth phase, marked by initial carbonate rock deposition; the Middle Miocene flourishing phase, characterized by extensive carbonate accumulation; and the Late Miocene submergence phase, where sedimentation slowed and the platform gradually submerged beneath the photic zone.

(3) The evolution of the Ganquan Platform is significantly influenced by various factors, including terrigenous clastic input, tectonic activity, variations in sea level, and the impact of paleomonsoons and paleocurrents. Specifically, the sea-level decline around 15 Ma, coupled with enhanced paleomonsoon activity, promoted the lateral growth of the platform. In contrast, the rapid rise in sea level at 8 Ma, combined with a notable

intensification of paleomonsoon influences, ultimately led to the submergence of the Ganquan Platform, profoundly altering its geomorphological characteristics.

References

1. Camoin, G.F.; Davies, P.J. *Reefs and Carbonate Platforms in the Pacific and Indian Oceans*; John Wiley & Sons: Hoboken, NJ, USA, 2009.
2. Read, J.F. Carbonate Platform Facies Models. *AAPG Bull.* **1985**, *69*, 1–21.
3. Hendry, J.; Burgess, P.; David, H.; Xavier, J.; Zampetti, V. Seismic characterization of carbonate platforms and reservoirs: An introduction and review. In *Seismic Characterization of Carbonate Platforms and Reservoirs*; Geological Society of London: London, UK, 2021.
4. Fauquembergue, K.; Mulder, T.; Reijmer, J.; Hanquiez, V.; Betzler, C.; Ducassou, E.; Recouvreur, A.; Principaud, M.; Borgomano, J.; Wilk, S.; et al. Sedimentology of Modern Bahamian Carbonate Slopes: Summary and Update. *Geochem. Geophys. Geosystems* **2024**, *25*, e2023GC011077. [CrossRef]
5. Alonso-Garcia, M.; Reolid, J.; Jimenez-Espejo, F.J. Sea-level and monsoonal control on the Maldives carbonate platform (Indian Ocean) over the last 1.3 million years. *Clim. Past Discuss.* **2023**, *2023*, 547–571. [CrossRef]
6. Haig, D.W.; Rigaud, S.; McCartain, E. Upper Triassic carbonate-platform facies, Timor-Leste: Foraminiferal indices and regional tectonostratigraphic association. *Palaeogeogr. Palaeoclimatol. Palaeoecol.* **2021**, *570*, 110362. [CrossRef]
7. Wu, S.; Zhang, X.; Yang, Z.; Wu, T.; Gao, J.; Wang, D. Spatial and Temporal Evolution of Cenozoic Carbonate Platforms on the Continental Margins of the South China Sea: Response to Opening of the Ocean Basin. *Interpretation* **2016**, *4*, 1–19. [CrossRef]
8. Wu, S.; Weilin, Z.; Yongsheng, M. Vicissitude of Cenozoic Carbonate Platforms in the South China Sea: Sedimentation in Semi-Closed Marginal Seas. *Mar. Geol. Quat. Geol.* **2018**, *38*, 1–17.
9. Eberli, G.P.; Masaferro, J.L.; Sarg, J.F. Seismic imaging of carbonate reservoirs and systems. *AAPG Mem.* **2004**, *81*, 169–183.
10. Yan, W.; Zhang, G.; Xia, B.; Zhang, L.; Yang, Z.; Lei, Z.; Yao, H. Seismic Characteristics and Development Patterns of Miocene Carbonate Platform in the Beikang Basin, Southern South China Sea. *Acta Geol. Sin. Engl. Ed.* **2020**, *94*, 1651–1661. [CrossRef]
11. Gao, H.; Zeng, X.; Liu, Z.; Bai, Z. Simulating of Subsidence History and Analysis of Tectonic Evolutionary Characteristics of Liyue Basin in South China Sea. *Geotecton. Metallog.* **2005**, *29*, 385–390.
12. Yao, Y.; Liu, H.; Yang, C.; Han, B.; Tian, J.; Yin, Z.; Gong, J.; Xu, Q. Characteristics and Evolution of Cenozoic Sediments in the Liyue Basin, SE South China Sea. *J. Asian Earth Sci.* **2012**, *60*, 114–129. [CrossRef]
13. Fyhn, M.B.; Boldreel, L.O.; Nielsen, L.H.; Giang, T.C.; Nga, L.H.; Hong, N.T.; Nguyen, N.D.; Abatzis, I. Carbonate Platform Growth and Demise Offshore Central Vietnam: Effects of Early Miocene Transgression and Subsequent Onshore Uplift. *J. Asian Earth Sci.* **2013**, *76*, 152–168. [CrossRef]
14. Tyrrell, W., Jr.; Christian, H., Jr. Exploration History of Liuhua 11-1 Field, Pearl River Mouth Basin, China. *AAPG Bull.* **1992**, *76*, 1209–1223.
15. Wu, S.; Yang, Z.; Wang, D.; Lu, F.; Lüdmann, T.; Fulthorpe, C.; Wang, B. Architecture, Development and Geological Control of the Xisha Carbonate Platforms, Northwestern South China Sea. *Mar. Geol.* **2014**, *350*, 71–83. [CrossRef]
16. Yang, Z.; Li, X.; Huang, L.; Wang, L.; Wu, S.; Zhang, X. Development of the Miocene Guangle Carbonate Platform in the South China Sea: Architecture and Controlling Factors. *Acta Geol. Sin. Engl. Ed.* **2021**, *95*, 177–191. [CrossRef]
17. Sattler, U.; Immenhauser, A.; Schlager, W.; Zampetti, V. Drowning History of a Miocene Carbonate Platform (Zhujiang Formation, South China Sea). *Sediment. Geol.* **2009**, *219*, 318–331. [CrossRef]
18. Shixiang, L.; Gongcheng, Z.; Zhigang, Z.; Xiaojun, X.; Long, W.; Shuang, S.; Jia, G.; Shenglan, W.; Yankun, B.; Yibo, W. Control of Tectonic Cycle in South China Sea over Hydrocarbon Accumulation in the Zengmu Basin. *China Pet. Explor.* **2016**, *21*, 37.
19. Yang, Z.; Zhang, G.; Liu, S.; Du, X.; Wang, L.; Yan, W.; Huang, L. Evolution and Controlling Factors of the Reef and Carbonate Platform in Wan'an Basin, South China Sea. *Appl. Sci.* **2022**, *12*, 9322. [CrossRef]

20. Aurelio, M.A.; Forbes, M.T.; Taguibao, K.J.L.; Savella, R.B.; Bacud, J.A.; Franke, D.; Pubellier, M.; Savva, D.; Meresse, F.; Steuer, S. Middle to Late Cenozoic Tectonic Events in South and Central Palawan (Philippines) and Their Implications to the Evolution of the South-Eastern Margin of South China Sea: Evidence from Onshore Structural and Offshore Seismic Data. *Mar. Pet. Geol.* **2014**, *58*, 658–673. [CrossRef]

21. Han, J.; Xu, G.; Li, Y.; Zhuo, H. Evolutionary History and Controlling Factors of the Shelf Breaks in the Pearl River Mouth Basin, Northern South China Sea. *Mar. Pet. Geol.* **2016**, *77*, 179–189. [CrossRef]

22. Zampetti, V.; Schlager, W.; van Konijnenburg, J.-H.; Everts, A.-J. Architecture and Growth History of a Miocene Carbonate Platform from 3D Seismic Reflection Data; Luconia Province, Offshore Sarawak, Malaysia. *Mar. Pet. Geol.* **2004**, *21*, 517–534. [CrossRef]

23. Betzler, C.; Hübscher, C.; Lindhorst, S.; Reijmer, J.J.; Römer, M.; Droxler, A.W.; Fürstenau, J.; Lüdmann, T. Monsoon-Induced Partial Carbonate Platform Drowning (Maldives, Indian Ocean). *Geology* **2009**, *37*, 867–870. [CrossRef]

24. Steuer, S.; Franke, D.; Meresse, F.; Savva, D.; Pubellier, M.; Auxietre, J.-L. Oligocene-Miocene Carbonates and Their Role for Constraining the Rifting and Collision Histroy of the Dangerous Grouds, South China Sea. *Mar. Pet. Geol.* **2013**, *30*, 1e14.

25. Betzler, C.; Eberli, G.P. Miocene Start of Modern Carbonate Platforms. *Geology* **2019**, *47*, 771–775. [CrossRef]

26. Yi, L.; Yuchi, C.; Xinyu, L. Formation Process and Controlling Factors of Carbonate Platform in Xisha Area, South China Sea: Based on Geochemical Evidences from Well Xike-1. *J. Palaeogeogr. (Chin. Ed.)* **2020**, *22*, 1197–1208.

27. Zhang, X.; Wu, S. Characteristics of Miocene Guangle Carbonate Platforms in the Xisha Area and Its Evolution. *Mar. Geol. Quat. Geol.* **2018**, *38*, 159–171.

28. Shao, L.; Li, Q.; Zhu, W.; Zhang, D.; Qiao, P.; Liu, X.; You, L.; Cui, Y.; Dong, X. Neogene Carbonate Platform Development in the NW South China Sea: Litho-, Bio-and Chemo-Stratigraphic Evidence. *Mar. Geol.* **2017**, *385*, 233–243. [CrossRef]

29. Shao, L.; Cui, Y.; Qiao, P.; Zhang, D.; Liu, X.; Zhang, C. Sea-Level Changes and Carbonate Platform Evolution of the Xisha Islands (South China Sea) since the Early Miocene. *Palaeogeogr. Palaeoclimatol. Palaeoecol.* **2017**, *485*, 504–516. [CrossRef]

30. Yubo, M.; Shiguo, W.; Fuliang, L.; Dongdong, D.; Qiliang, S.; Yintao, L.; Mingfeng, G. Seismic Characteristics and Development of the Xisha Carbonate Platforms, Northern Margin of the South China Sea. *J. Asian Earth Sci.* **2011**, *40*, 770–783. [CrossRef]

31. Liu, Y.; Wu, S.; Li, X.; Chen, W.; Han, X.; Yang, C.; Qin, Y.; Huang, X.; Yang, Z.; Sun, J. Seismic Stratigraphy and Development of a Modern Isolated Carbonate Platform (Xuande Atoll) in the South China Sea. *Front. Earth Sci.* **2023**, *10*, 1042371. [CrossRef]

32. Wu, S.; Chen, W.; Huang, X.; Liu, G.; Li, X.; Betzler, C. Facies Model on the Modern Isolated Carbonate Platform in the Xisha Archipelago, South China Sea. *Mar. Geol.* **2020**, *425*, 106203. [CrossRef]

33. Wu, S.; Zhang, H.; Qin, Y.; Chen, W.; Liu, G.; Han, X. Seismic Imaging and 3D Architecture of Yongle Atoll of the Xisha Archipelago, South China Sea. *Acta Geol. Sin.-Engl. Ed.* **2022**, *96*, 1778–1791. [CrossRef]

34. Li, X.; Guo, X.; Tian, F.; Fang, X. The Effects of Controlling Gas Escape and Bottom Current Activity on the Evolution of Pockmarks in the Northwest of the Xisha Uplift, South China Sea. *J. Mar. Sci. Eng.* **2024**, *12*, 1505. [CrossRef]

35. Briais, A.; Patriat, P.; Tapponnier, P. Updated Interpretation of Magnetic Anomalies and Seafloor Spreading Stages in the South China Sea: Implications for the Tertiary Tectonics of Southeast Asia. *J. Geophys. Res. Solid Earth* **1993**, *98*, 6299–6328. [CrossRef]

36. Li, C.; Li, J.; Ding, W.; Franke, D.; Yao, Y.; Shi, H.; Pang, X.; Cao, Y.; Lin, J.; Kulhanek, D.; et al. Seismic Stratigraphy of the Central South China Sea Basin and Implications for Neotectonics. *J. Geophys. Res. Solid Earth* **2015**, *120*, 1377–1399. [CrossRef]

37. Yan, Q.; Shi, X.; Castillo, P.R. The Late Mesozoic–Cenozoic Tectonic Evolution of the South China Sea: A Petrologic Perspective. *J. Asian Earth Sci.* **2014**, *85*, 178–201. [CrossRef]

38. Sun, Z.; Zhou, D.; Zhong, Z.; Zeng, Z.; Wu, S. Experimental Evidence for the Dynamics of the Formation of the Yinggehai Basin, NW South China Sea. *Tectonophysics* **2003**, *372*, 41–58. [CrossRef]

39. Wang, H.; Zhao, Q.; Wu, S.; Wang, D.; Wang, B. Post-Rifting Magmatism and the Drowned Reefs in the Xisha Archipelago Domain. *J. Ocean. Univ. China* **2018**, *17*, 195–208. [CrossRef]

40. Luo, W.; Zhang, D.; Liu, X.; Wang, Z.; Hu, W.; Wang, Y. A Comprehensive Stratigraphic Study of Well XK-1 in the Xisha Area. *J. Stratigr.* **2018**, *42*, 485–498.

41. Sun, J. A Discussion on the Formation Ages of the Bedrock in the Xisha Islands. *Mar. Geol. Quat. Geol.* **1987**, *7*, 5–6.

42. Gao, J.; Bangs, N.; Wu, S.; Cai, G.; Han, S.; Ma, B.; Wang, J.; Xie, Y.; Huang, W.; Dong, D. Post-seafloor Spreading Magmatism and Associated Magmatic Hydrothermal Systems in the Xisha Uplift Region, Northwestern South China Sea. *Basin Res.* **2019**, *31*, 688–708. [CrossRef]

43. Wan, S.; Li, A.; Clift, P.D.; Stuut, J.-B.W. Development of the East Asian Monsoon: Mineralogical and Sedimentologic Records in the Northern South China Sea since 20 Ma. *Palaeogeogr. Palaeoclimatol. Palaeoecol.* **2007**, *254*, 561–582. [CrossRef]

44. Xie, X.; Müller, R.D.; Ren, J.; Jiang, T.; Zhang, C. Stratigraphic Architecture and Evolution of the Continental Slope System in Offshore Hainan, Northern South China Sea. *Mar. Geol.* **2008**, *247*, 129–144. [CrossRef]

45. Haq, B.U.; Hardenbol, J.; Vail, P.R. Chronology of Fluctuating Sea Levels since the Triassic. *Science* **1987**, *235*, 1156–1167. [CrossRef] [PubMed]

46. Miller, K.G.; Browning, J.V.; Schmelz, W.J.; Kopp, R.E.; Mountain, G.S.; Wright, J.D. Cenozoic Sea-Level and Cryospheric Evolution from Deep-Sea Geochemical and Continental Margin Records. *Sci. Adv.* **2020**, *6*, 1346. [CrossRef]

47. Chen, W.; Wu, S.; Wang, D.; Betzler, C.; Ma, Y. Stratigraphic Evolution and Drowning Steps of a Submerged Isolated Carbonate Platform in the Northern South China Sea. *Front. Mar. Sci.* **2023**, *10*, 1200788. [CrossRef]

48. Sarg, J.F. The sequence stratigraphy, sedimentology, and economic importance of evaporite–carbonate transitions: A review. *Sediment. Geol.* **2001**, *140*, 9–34. [CrossRef]

49. Du, W.; Yang, C.; Zhang, H.; Gao, J.; Wen, M.; Hu, X.; Xu, Z.; Nie, X.; Zhu, R. First Documentation of Large Submarine Sinkholes on the Ganquan Carbonate Platform in the Xisha Islands, South China Sea. *J. Mar. Sci. Eng.* **2023**, *11*, 2171. [CrossRef]

50. Zhu, W.; Xie, X.; Wang, Z.; Zhang, D.; Zhang, C.; Cao, L.; Shao, L. New Insights on the Origin of the Basement of the Xisha Uplift, South China Sea. *Sci. China Eatrh Sci.* **2017**, *60*, 2214–2222. [CrossRef]

51. Qin, Y.; Wu, S.; Betzler, C. Backstepping Patterns of an Isolated Carbonate Platform in the Northern South China Sea and Its Implication for Paleoceanography and Paleoclimate. *Mar. Pet. Geol.* **2022**, *146*, 105927. [CrossRef]

52. Anselmetti, F.S.; Eberli, G.P.; Ding, Z.-D. From the Great Bahama Bank into the Straits of Florida: A Margin Architecture Controlled by Sea-Level Fluctuations and Ocean Currents. *Geol. Soc. Am. Bull.* **2000**, *112*, 829–844. [CrossRef]

53. Lüdmann, T.; Betzler, C.; Eberli, G.P.; Reolid, J.; Reijmer, J.J.; Sloss, C.R.; Bialik, O.M.; Alvarez-Zarikian, C.A.; Alonso-García, M.; Blättler, C.L. Carbonate Delta Drift: A New Sediment Drift Type. *Mar. Geol.* **2018**, *401*, 98–111. [CrossRef]

54. Betzler, C.; Eberli, G.P.; Kroon, D.; Wright, J.D.; Swart, P.K.; Nath, B.N.; Alvarez-Zarikian, C.A.; Alonso-García, M.; Bialik, O.M.; Blättler, C.L. The Abrupt Onset of the Modern South Asian Monsoon Winds. *Sci. Rep.* **2016**, *6*, 29838. [CrossRef] [PubMed]

55. Shiming, W.; Anchun, L.; Kehui, X.; Xueming, Y. Characteristics of Clay Minerals in the Northern South China Sea and Its Implications for Evolution of East Asian Monsoon since Miocene. *J. China Univ. Geosci.* **2008**, *19*, 23–37. [CrossRef]